

pubs.acs.org/JPCB Article

Quantitative Evidence of Mobile Ion Hopping in Polymerized Ionic Liquids

Published as part of The Journal of Physical Chemistry virtual special issue "Lawrence R. Pratt Festschrift". Hongjun Liu, Xubo Luo, Alexei P. Sokolov, and Stephen J. Paddison*



Cite This: J. Phys. Chem. B 2021, 125, 372-381



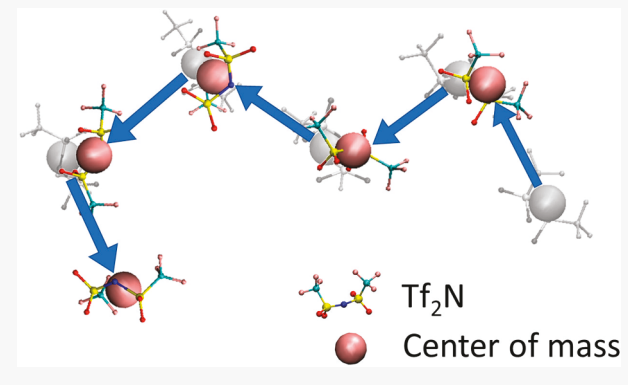
ACCESS

Metrics & More

Article Recommendations

Supporting Information

ABSTRACT: Atomistic molecular dynamics simulations were performed, and an extensive set of analyses were undertaken to understand the ion transport mechanism in the polymerized ionic liquid $poly(C_2VIm)Tf_2N$. The ion hopping events were investigated at different time scales. Ion hopping was examined by monitoring the instantaneous cation—anion association and dissociation. Ion diffusion was subsequently evaluated with correlation functions and the calculation of relaxation times at different time scales. Dynamical heterogeneity in the mobility of the ions was observed with only a small portion of the anions classified as fast mobile ions. The mobile ions were characterized as the ones traveling farther than a certain distance during a characteristic period, which was much longer than the time scale of the instant ion pair dissociation. Effective hopping of



the mobile ions contributed to the diffusivity which was dominated by interchain hopping and generally facilitated with five associating cations from two different polymer chains. Mobile anions had relatively fewer associating cations from more associating chains than immobile anions. The stringlike cooperative motion was observed in the mobile anions. The string length was determined to decrease with increasing temperature. These findings provided an in-depth understanding of the ion transport in polymerized ionic liquids and important information for the rational design of novel materials.

INTRODUCTION

Polymerized ionic liquids (polyILs) are polymers containing ionic liquid moieties in each monomer. These materials combine the ion transport behavior of an ionic liquid with the favorable mechanical properties of a polymer. This promises or at least provokes the possibility of polyILs as a new class of electrolytes for electrochemical devices. However, the typical ionic conductivity of a polyIL is considerably lower than observed in low molecular weight ionic liquids,³ which has thus far hindered the wide application of polyILs.^{4–8} To rationally design polyILs with promising conductivity, it is essential to uncover a fundamental understanding of the mechanisms of ion transport.9-14 The low ion conductivity was attributed to the elevated glass transition temperature and the depleted number of mobile ions after covalently bonding the ions to polymer backbones. 15 However, the ion transport in polyILs is more complicated than suggested by the above description. Recent experimental studies have unveiled the decoupling of conductivity from the segmental dynamics in polyILs, which has been observed below the glass transition temperature and within the superionic regime with a Walden plot. 12,16-18 Moreover, recent investigations into the strongly correlated motion in polyILs provoked the hypothesis of the existence of closed loops of the counterions. Specifically, ionic conductivity was observed

to be significantly slower than ion diffusion, which was quantified by an unusually low inverse Haven ratio. ^{18,19}

In addition to these experimental studies, a clear description of ion transport is warranted at the molecular level. Molecular dynamics (MD) simulations pose an indispensable avenue and tool for tackling this issue. ^{20–23} A pioneering communication by Ganesan et al. utilized MD simulations to investigate the mechanism of ion transport in polyILs. ²³ Ion hopping occurs when a counterion loses an existing association with a polymerized ionic group or forms a new association. This research group found a correlation between diffusivity and the average lifetime of ion association. Hopping events were then categorized into intrachain, interchain, and chain-to-free hopping events, which were defined only from the identities of the polymerized ionic groups associated with the targeted counterion. It was pointed out that the intrachain hopping of the

Received: July 28, 2020 Revised: December 10, 2020 Published: January 4, 2021





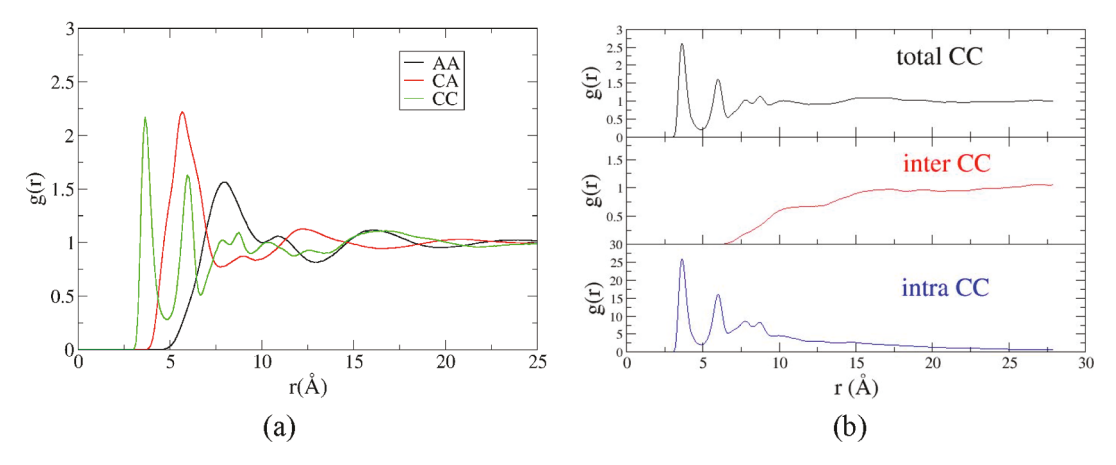


Figure 1. Center-of-mass radial distribution function, g(r), between the imidazolium rings of the cations (C) and anions (A). (a) Overall g(r). (b) Decomposition of CC g(r). The out-of-phase correlation between like ions and unlike ions is evident. Four short distance CC peaks below 10 Å are solely of a polymer nature and due to the chain connectivity

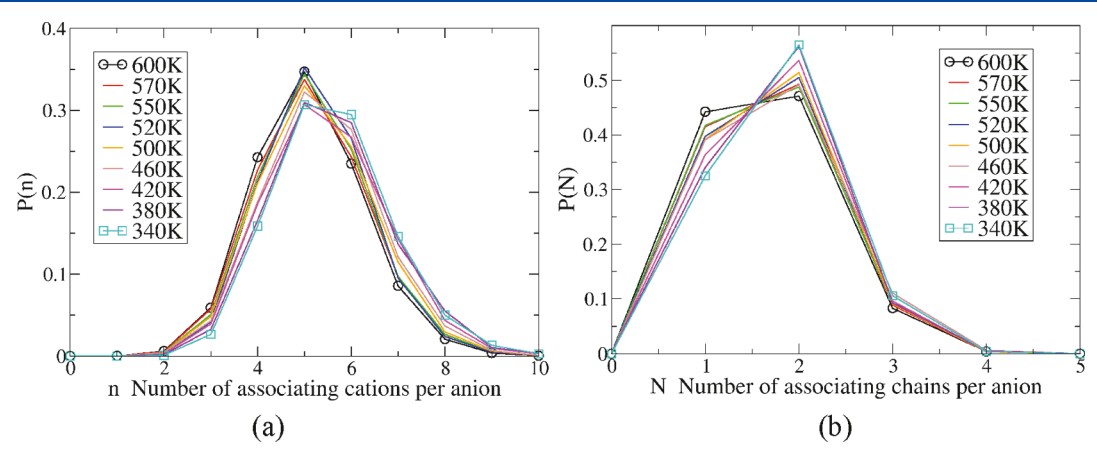


Figure 2. Temperature effect on ion coordination: P(n) is the probability of an anion associating with n cations, and P(N) is the probability of an anion associating with N chains. An increase in the temperature shifts P(n) and P(N) distributions to the left. On average, one anion coordinates with 4, 5, or 6 cations from 1 or 2 polycation chains.

anions was identified to be the dominant mode of ion transport in polyILs. This method of analysis was subsequently employed for various polyILs, ^{24–29} which provided very useful information for the rational design of novel materials. However, the existing definition of ion hopping was limited to ion association and dissociation, which does not capture the exact motion of a single ion. Thus, we advocate that the methodology can be improved to elucidate a more complete picture. Specifically, the presence of dynamical heterogeneity and stringlike motion are important and worth examining. Prior work has witnessed these phenomena in ionic liquids (ILs). ^{30–34} Cooperative motion of the ions was also observed in molecular simulations of polymeric single-ion conductors. ^{35,36} Thus, we assert that the dynamical heterogeneity and stringlike motion could also be present in these polymerized systems and are therefore an important thrust of this investigation.

Motivated by the aforementioned studies, MD simulations were undertaken with poly(n-ethylvinylimidazolium) bistrifluoromethylsulfonylimide) $[poly(C_2VIM)Tf_2N]$ at various temperatures. To find the quantitative evidence of mobile ion hopping, a series of analyses were performed, including ion association, diffusivity, categorization of hopping, dynamical heterogeneity, and stringlike cooperative motion. We submit that our results will extensively broaden the community's understanding of the mechanism of ion transport in polyILs and

thereby potentially guide the development of such a class of materials.

SIMULATIONS

The simulation setup and the force field parameters employed in the present work are identical with our prior studies, and the reader is referred to them for a complete description.^{37,38} Only important points needed for clarity are provided here: the simulated system consisted of 10 polycation chains made up of 40 monomers and 400 anions, resulting in a total number of 14020 atoms. The general Amber force field (GAFF) was used for the bonded and nonbonded interactions.³⁹ A cutoff distance of 14 Å was used in the Lennard-Jones interactions with the appropriate tail corrections and electrostatic interactions with the particle mesh Ewald (PME) method. Information for the input files was directly taken from the initial configurations from our prior work as eluded to above.³⁷ Trajectories of 300 ns were collected over a range of different temperatures, which were set above the experimental glass transition temperature. 7,40,41 All molecular dynamics (MD) simulations were performed with the GROMACS package.⁴²

■ RESULTS AND DISCUSSION

Structural and Ion Association Analysis. A structural analysis was first performed prior to the investigation of the

dynamics. Center-of-mass radial distribution functions, g(r), between the imidazolium ring of the cations, C, and anions, A, are displayed in Figure 1. The out-of-phase correlation between like ions and unlike ions is evident. It is a ubiquitous characteristic for any ionic system since the local electroneutrality must be fulfilled. Four short distance CC peaks below 10 Å are solely of polymer nature and due to the intrachain connectivity, which can be seen in the comparison of the total CC g(r) and intrachain CC g(r). Because the intrachain cations are constrained by covalent bonds to the polymer, the spatial distribution of the neighboring intrachain cations is further investigated and is shown in Figure S1. The first neighboring cations prefer distances of 3.5 and 6 Å, along with the dihedral orientations of 25° and 105°, respectively. The second neighboring cations present more evenly distributed orientations due to the longer connecting backbone, which have the preferred orientations of 40°, 105°, and 135°.

Ion association is defined with a cutoff distance of 7.8 Å, which is the first local minimum of the CA g(r). If the distance between the cations and anions is smaller than this cutoff, the ions are deemed as associated or coordinated. The probabilities of an anion associating with n cationic groups or with N polymer chains are denoted P(n) and P(N), respectively. The statistical results are presented in Figure 2 at each of the selected temperatures (i.e., 340-600 K). Each anion generally associates with 4, 5, or 6 cations from 1 to 3 chains. Increasing the temperature shifts the associating cation distribution, P(n), and coordinating chain distribution, P(N), to the left; thus, each anion coordinates with fewer cations and chains at higher temperatures. To obtain a visual sense of the ion association, inspection was made of snapshots taken from the simulation trajectories. The "half-shell" coordination is easy to locate, as shown in Figure S2, where the associated cations do not form a closed coordination cage. This could be attributed to the constraints on the polymerized cations by the backbone, as depicted in Figure 1b and Figure S1. In the open directions of the coordination, there are cations outside the first minimum of the CA g(r), i.e., not defined as associated. However, these cations are not far away from the targeted anion, which could increase association as the time elapses. Thus, this "half-shell" coordination and the unassociated cations that are in close proximity might be regarded as being in a "loose cage".

Categorization of Ion Hopping. The categorization of the ion hopping events is based on the identities of the associated cationic group, similar to the work of Ganesan et al.²³ The present work revises and improves the definitions, identifying four distinct types which are sketched in Figure 3: type 1, intrachain hopping; type 2, interchain hopping; type 3, hopping involving nonassociating free anions; and type 4, intact (rattling). Introducing the type 4 distinguishes the ions intact from the others, which avoids the artificial inflation of intrachain/interchain hopping into the statistics. In the numerical implementation, every anion has a list of associating cations, termed the "cation list". It also has a "chain list" of the polymer chains containing the associating cations. The cation list may gain or lose entities as the time elapses from t = 0 to t = Δt , where Δt is the sampling time interval, as well as the chain list. If the cation list does not change, the anion is counted as type 4. If the cation list is empty at Δt , it is type 3. If only the cation list changes, i.e., the anion gains or loses an associating cation but is still associating with the same polymer chain(s), it is type 1. If both the cation and chain lists change, it is categorized as type 2. We recognize that the fastest hopping events take place

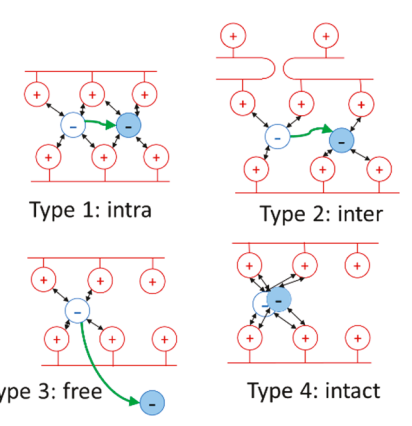


Figure 3. Categorization of the types of ion hopping. Green arrows denote anion movement from t = 0 (open blue circles) to $t = \Delta t$ (filled blue circles). Black arrows indicate ion associations. The hopping events can be identified as type 1 (intrachain), type 2 (interchain), type 3 (involving nonassociating free anions), and type 4 (remaining intact and hence only rattling).

at a subpicosecond time scale according to Ganesan et al. 23 However, their investigation has proved that resolutions of 10^0 – 10^2 ps have no qualitative deviations. A test in Figure S3 also shows the possibility of using a large sampling time. Thus, sampling at intervals of 10 ps was chosen for the convenience of computational cost.

Figure 4a shows the percentages of the four types. Intrachain hopping is about 30–40% of the total, which is always more than interchain hopping. Type 3 is essentially zero. A substantial percentage of type 4 is observed, making up about 35–50%, which means that a considerable number of anions do not experience the breaking or forming of association. Increasing the temperature promotes both intrachain and interchain hopping, but the curve becomes more concave, indicating more enhancement on the interchain hopping. Figure 4b gives the details of intrachain hopping that the majority of intrachain hopping involve one or two chains. The probability of involving only one chain in the intrachain hopping events increases with temperature, while those involving more chains decrease.

Effect of Structural and Ion Association Relaxation on Diffusivity. The diffusivity is calculated from the mean square displacement (MSD) of the anions with the Einstein relation. MSD plots at different temperatures are shown in Figure S4a. Sluggish dynamics is evident at the lowest temperatures, and hence, $D_{\rm Anion}$ can only be reliably derived in the diffusive regime, which is captured at the temperatures above 420 K. With an ultrafine sampling time (Figure S4b), a plateau in the MSD is observed at about 1–100 ps. This plateau implies that ion motion at such a short time scale does not contribute to the diffusion, which is attributed to the rattling of the anions in the cage formed by the surrounding cations. The computed $D_{\rm Anion}$ is found to underestimate the dynamics in comparison to the experimental data (Figure S5), which is common in molecular simulations of ILs and polyILs. 29,31,43

To investigate the relation of diffusion to structural relaxation and ion association, the self-intermediate scattering function, $F_s(q,t)$, intermittent time correlation function, C(t), and continuous time correlation function, S(t), were calculated. The self-intermediate scattering function only represents the motion of the anions regardless of the cation—anion association, which is calculated with $F_s(q,t) = \langle \exp(i\mathbf{q}\cdot[\mathbf{r}_i(t)-\mathbf{r}_i(0)])\rangle$, where \mathbf{q} is the reciprocal wave vector and $q = |\mathbf{q}|$. The wavevector

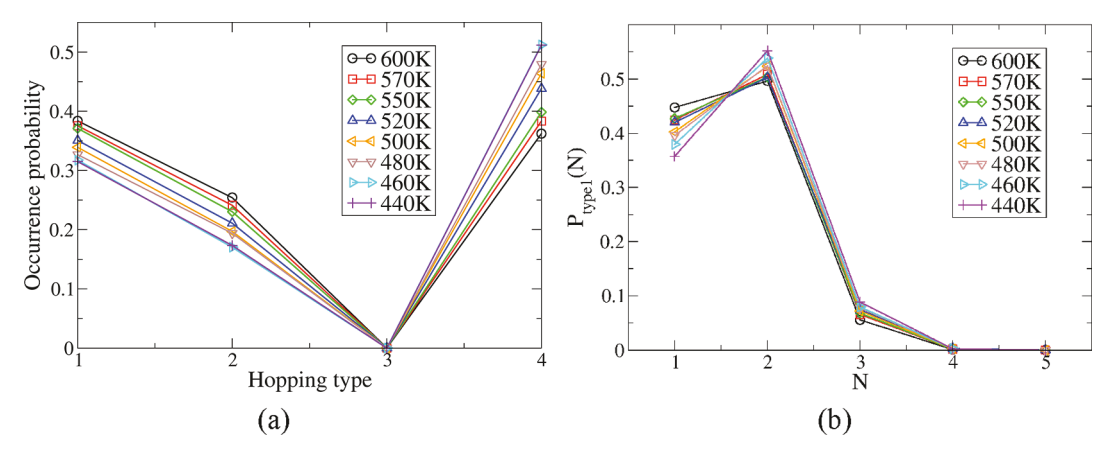


Figure 4. Temperature effect on occurrence probability of ion hopping types at a time resolution of 10 ps. (a) Hopping types. (b) Chain association of the anions experiencing intrachain hopping. *N* is the number of associated chains in type 1 hopping.

 $q^* = 0.76 \text{ Å}^{-1}$ is chosen for $F_s(q^*,t)$, which corresponds to the first peak of the AA g(r) in real space.³¹ A test of q values is in Figure S6 as supplementary. S(t) and C(t) are calculated with $S(t) = \langle H(t)h(0)\rangle/\langle h\rangle$ and $C(t) = \langle h(t)h(0)\rangle/\langle h\rangle$, respectively, where h(t) is unity if an ion association is presented at time t, and H(t) has a value of unity if the ion association at t = 0 remains intact continuously up to time t; otherwise, h(t) and H(t) are zero. S(t) decays with the initial breaking of the cation—anion association, but C(t) decays only when the anion finally dissociates from the anion without recovery. Conceptually, the time scale of S(t) is comparable to the hopping categorization in Figure 4 because both quantities reflect the instant breaking of the ion pair association. As anticipated, S(t) decays faster with a shorter sampling time and relaxes more rapidly than C(t) as clearly seen in Figure S7. The structural relaxation times, τ_q , τ_c , and the ion association lifetime, τ_s , are extracted from $F_s(q,t)$, C(t), and S(t), respectively, ⁴⁴ Practically, the relaxation time is calculated by fitting the time correlation function to a stretched exponential function and analytically integrated.^{24,27,44} To ensure acceptable quality, $au_{\rm q}$ and $au_{\rm c}$ were calculated over the entire 300 ns of trajectory as they are independent of the sampling frequency, while τ_s is calculated from a trajectory that is long enough for S(t) to decay below 0.2.

Figure 5 plots the diffusivity as a function of relaxation time, and the data points are fitted to the power law $D \sim \tau^{-\lambda}$. The fitted curves reveal that λ is approximately equal to 1 for $\tau_{\rm c}$ but distinct from unity for $\tau_{\rm q}$ or $\tau_{\rm s}$. The linear correlation of the diffusivity and $1/\tau_{\rm c}$ seems to be in contradiction to the pioneering work of Ganesan et al., where they demonstrated the relation $D \sim \tau_{\rm s}^{-1}$. However, this issue of $D \sim \tau^{-\lambda}$ is rather complicated. Subsequent work by Ganesan and coauthors also observed $D \sim \tau_{\rm s}^{-1}$, or $D \sim \tau_{\rm c}^{-1}$, or both the $D \sim \tau_{\rm s}^{-1}$ and $D \sim \tau_{\rm c}^{-1}$ for various polyILs with different cations. Also expected that $D \sim \tau_{\rm s}^{-1}$ is a coarse-grained simulation of ionic polymers. As our results do not confirm these earlier findings, this issue is not definitively settled.

Dynamical Heterogeneity. The observations discussed above raise the following question: does the ion hopping, as defined, contribute to the diffusion? Ion hopping was only defined on the basis of the ion pair dissociation, and a considerable contribution of intra- and interchain hopping was observed every 10 ps. The MSD, however, has a plateau at the time scale of $1{\text -}100$ ps, indicating a nondiffusive regime at this time scale. $D \sim \tau_c^{-1}$ implies that the diffusion is correlated to dissociation of the ion pair followed by the eventual departure

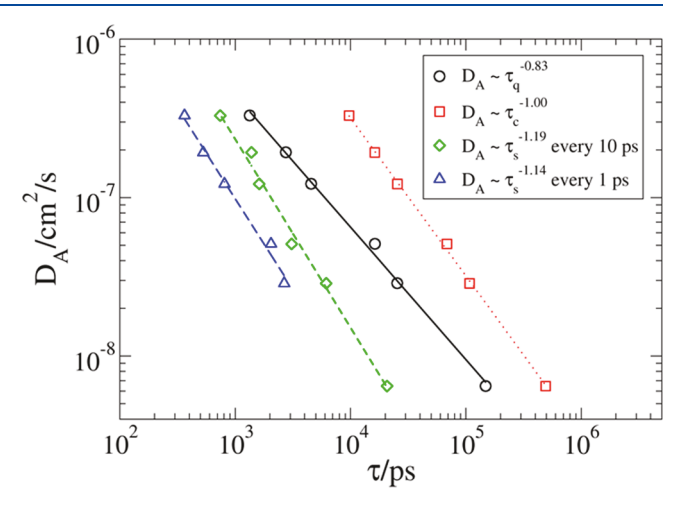


Figure 5. Correlation between anion diffusivity and relaxation time. The ion association relaxation $\tau_{\rm s}$ is probed by the continuous time autocorrelation function S(t). Structural relaxation times $\tau_{\rm q}$ and $\tau_{\rm c}$ are characterized by the self-intermediate scattering function and intermittent time autocorrelation function, respectively.

from the "cation cage". This phenomenon happens at time scales much longer than the hopping categorization or the decay of S(t). To resolve this problem, an analysis over a longer time scale is required. The self-part of the van Hove function, $G_s(r,t) = (1/r^2)^{-1}$ $N)\sum_{i=1}^{N}\langle\delta(r-|\mathbf{r}_{i}(t)-\mathbf{r}_{i}(0)|)\rangle$, was investigated for the anions, where δ is the Kronecker delta. $G_s(r,t)$ characterizes the dynamical heterogeneity by its deviation from ideal Gaussian behavior, i.e., $G_{s,0}(r,t) = \left(\frac{3}{2}\langle r^2(t)\rangle\right)^{3/2} \exp\left(-\frac{3r^2}{2}\langle r^2(t)\rangle\right)$ $^{.46-48}$ The degree of deviation is quantified by the non-Gaussian parameter: $\alpha_2 = \frac{3\langle (r(t) - r(0))^4 \rangle}{5\langle (r(t) - r(0))^2 \rangle^2} - 1$. In Figure 6, the characteristic time scale t^* is defined as the time it takes for α_2 to reach its maximum; that is, $\alpha_2(t^*) = \alpha_2^{\text{max}}$, which is the time that dynamical heterogeneity is the greatest. The maximum in α_2 generally decreases with temperature, and t^* exhibits a similar trend. Dynamic heterogeneity is a universal property of condensed liquids, well established in glass-forming or supercooled liquids, ^{46,47} polymer melts, ⁴⁹ lipid membranes, ^{50,51} polymer films, ⁵² proteins, ⁴⁸ and ionic liquids. ³¹ Compared with low molecular weight ionic liquids, polyILs exhibit greater dynamical heterogeneity. At $T \le 460$ K, the α_2^{max} of the polyILs in this work reaches values greater than 1.5. In the similar case

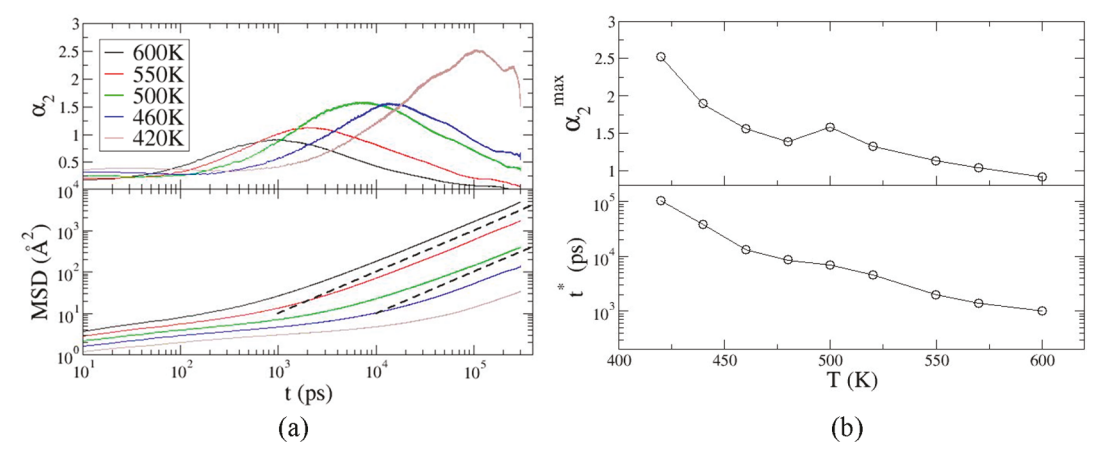


Figure 6. (a) Mean-squared displacement (MSD) and the non-Gaussian parameters (α_2) for the anions. (b) Maxima of α_2 and the corresponding time scale t^* . The dashed lines in the MSD are for a slope of one, indicating diffusive behavior. The maxima of α_2 and t^* quantify the degree and time scale of the strongest dynamical heterogeneity, both of which decrease with temperature.

with the low molecular weight ionic liquids and the Tf_2N^- anion, the α_2^{max} was observed to be lower than 0.5. ^{53,54} This difference may be due to the solid state material and the polymerized cations of the polyIL.

The function of $4\pi r^2 G_s(r,t)$ evaluates the probability distribution of the anions traveling to the distance of r in time t. An initial calculation in Figure S8 estimates that 97% of the anions do not travel far enough to leave their original cage in 10 ps. Thus, the hopping events should be investigated at a longer time scale, such as t^* , and a distance criterion is proposed to ensure the hopping is effective. Figure 7 shows the $G_s(r,t^*)$ at the

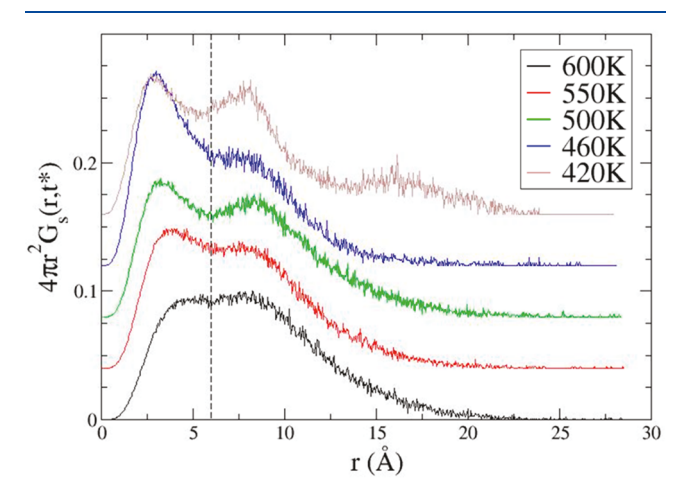


Figure 7. Self-part of the van Hove function, $G_s(r,t^*)$, at different temperatures. For clarity, each $G_s(r,t^*)$ curve is vertically shifted by 0.02. The local minimum, $r^* = 6$ Å (vertical dashed line), is used to conveniently distinguish two populations (fast and slow) of anions. Multiple peaks in $G_s(r,t)$ are a signature of hopping motion of the anions to preferentially quantized distances.

characteristic time of the maximum dynamical heterogeneity. The temperature dependence and time dependence of $G_s(r,t)$ are shown in Figure S9. The occurrence of a secondary peak in $G_s(r,t^*)$ is a quantitative signature of hopping diffusion. The first peak (r < 6 Å) suggests the anion of interest is exploring the original coordination cage. The second peak at about 8 Å is consistent with the first peak of the AA g(r) and implies that the anion hops to the first neighboring cage. Hence, the local minimum of $G_s(r,t^*)$ at $r^* = 6 \text{ Å}$ is a natural distance criterion to

conclusively distinguish the fast "mobile" anions from the slow "immobile" ones. Mobile anions are the anions that have moved farther than the distance of r^* within time of t^* , while immobile anions stay inside the r^* range. There are other ways to dictate r^* to define mobile entities, such as $G_s(r^*,t^*) = G_0(r^*,t^*)$, ⁴⁶ or fitting of $G_s(r,t^*)$ as a superposition of two distinct mobility groups, ⁵⁰ or arbitrarily choosing the fastest 6% of the ions with the largest displacement. ⁵⁵ These different definitions reflect the freedom in defining the fast mobile ions. To corroborate the hopping peaks observed in the $G_s(r,t)$, the distinct part of the van Hove function, $G_d(r,t) = (1/N) \sum_{j\neq 1}^{N} (\delta(r - |\mathbf{r}_i(t) - \mathbf{r}_j(0)|) \rangle$, is calculated in Figure S10. The result dictates that the original positions are occupied by other anions at a later time and the anions present the concerted motion. $G_d(r,t)$ for the mobile anions in Figure S11 also seems to hint at a stronger cross-correlation

In distinguishing the types of mobile ions, it is necessary to review the interchain and intrachain hopping in Figure 3. The "half-shell" coordination and the "loose cage" might allow the anion to rattle with wider fluctuations involving temporary association and dissociation. This type of rattling has been identified as type 1 or type 2 hopping but rarely contributes to the diffusion of the ions. Hence, it is necessary to distinguish "effective hopping" from all the hopping events of ion pair dissociation. As illustrated in Figure 8, the effective hopping happens when the anion breaks its association and, meanwhile, travels farther than r^* to the neighboring cage by the time t^* . Otherwise, the hopping is ineffective. The discussion above implies that ion pair dissociation occurs frequently, but only a few of these events result in effective hopping at a longer time scale. Ion diffusion is a macroscopic property of effective hopping, and the distance criterion applies to both type 1 and type 2. The categorization of the effective intra- and interchain hopping is given in the following section along with the status of mobile ion association.

Local Environment of Mobile/Immobile Anions. Snapshots of the mobile anions are shown in Figure 9 and clearly demonstrate the spatial distribution of the mobile anions, suggesting a more isotropic spatial distribution at higher temperatures but more anisotropic at lower temperature. The stringlike cooperative motion of the mobile anions is seemingly visible at lower temperatures, which will be discussed later. The identity variation of the mobile anions and probability distribution of the number of mobile anions are presented in

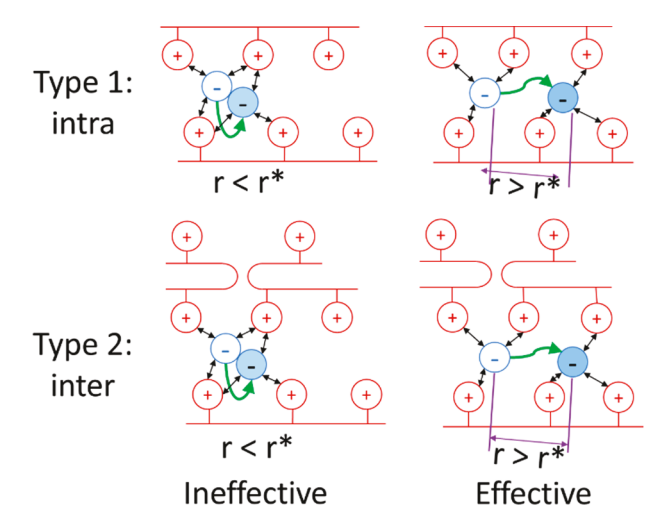


Figure 8. Illustration of effective hopping. The hopping events satisfying $r > r^*$ (right) effectively contribute to the diffusion. In contrast, ion dissociation (left) is not sufficient for movement of the ion.

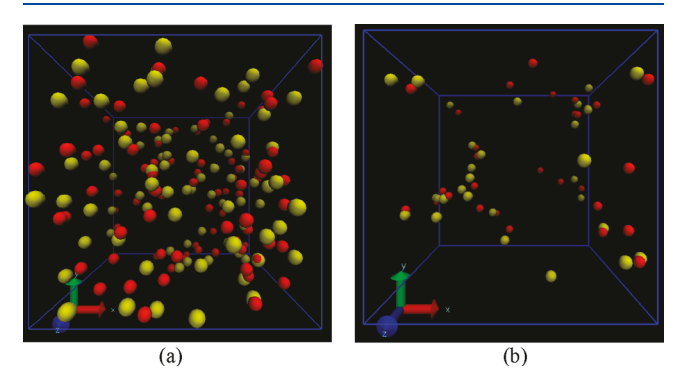


Figure 9. Spatial distribution of mobile anions at (a) 600 K and (b) 500 K. Yellow and red spheres are the anions at t = 0 and t^* , respectively. An isotropic spatial distribution is observed at higher temperature with more anisotropy occurring at the lower temperature.

Figure 10. Identities of the mobile anions constantly change during the simulations. Every single anion has approximately an equal probability to be mobile at higher temperatures, while the solidification of identity is detectable at lower temperatures, e.g., 440 and 420 K, where only a small percentage of the anions are mobile over the entire simulation. The number of mobile anions

constitute around 15% of the total anions at 600 K, but only 8% at 420 K. Hence, only a small percentage of anions are mobile on this time scale.

Because a large proportion of the anions are the slow ones not contributing to the ion transport at $t = t^*$, it is necessary to compare the ion association between the mobile ions and slow immobile ions. Figure 10 reveals that the mobile anions have relatively fewer associating cations from more associating chains than the immobile ions. This intuitive insight suggests that the more flexible coordination constraint leads to faster mobility. Figure 12 shows the categorization of the effective hopping events for only mobile anions and the probability mass function of hopping for mobile anions mediated by N chains. Thus, it only counts the mobile ions for effective hopping, and the ineffective hopping in the left panel of Figure 8 is excluded. It should be pointed out that the analysis in Figure 12 uses the time interval of t^* , which is an order of magnitude larger than the interval of only 10 ps previously utilized. The cutoff distance is 7.8 Å, the same as shown in Figure 4. One can conclude that the hopping of mobile anions is predominantly type 2 (i.e., interchain) and generally facilitated by five associating cations from two distinct chains. Type 1 intrachain hopping is a minor contributor and only accounts for about 15%, in contrast to categorization with a short sampling time interval as previously shown in Figure 4. Intrachain hopping of mobile anions is usually mediated by one or two associating chains, while interchain hopping is generally facilitated by a larger number of associating chains. The coordination environment varies little before and after interchain hopping. There is virtually no type 3 and a negligible amount of type 4 events. A decrease in temperature leads slightly to an enrichment of interchain hopping at the expense of intrachain ones, and both interchain and intrachain hopping involve more associating chains at lower temperature.

Stinglike Cooperative Motion. To quantify the number of mobile anions or string length (n_s) involved in the stringlike cooperative motion, the distance between each pair of mobile anions was examined over a certain time interval. Two anions belong to the same string if they satisfy $\min[|\mathbf{r}_i(t) - \mathbf{r}_j(0)|, \mathbf{r}_i(0) - \mathbf{r}_j(t)|] < r_s$, where $\mathbf{r}_i(t)$ and $\mathbf{r}_j(t)$ are the positions of the ith and jth anions at time t, and r_s is the cutoff distance determining the string connection. The characteristic time, t^* , is used to detect the stringlike motion, and a cutoff of 2.5 Å is a little larger than the "hard core" radius of the anions, i.e., $t = t^*$ and $r_s = 2.5$ Å in

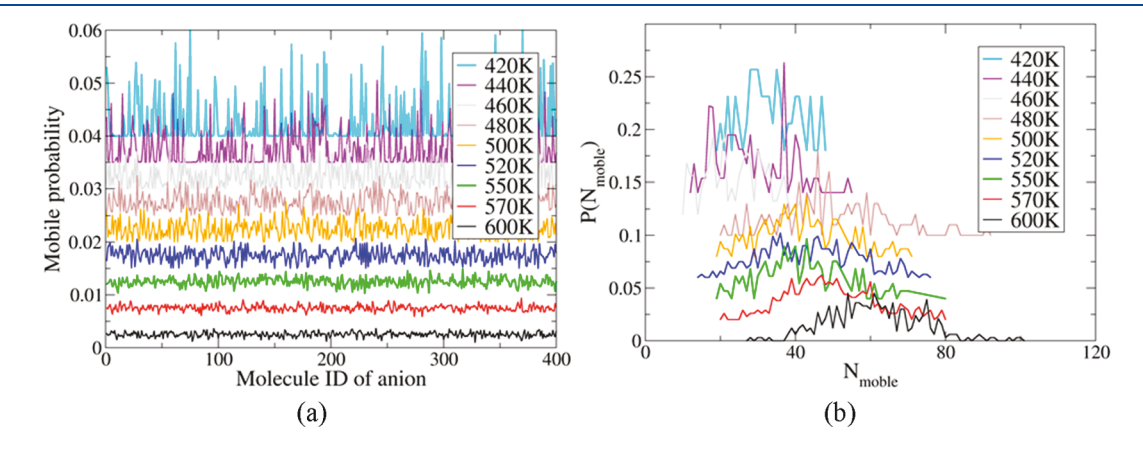


Figure 10. Variation in the identity of mobile anions at each temperature: (a) the mobile probability mass function vs the identity of the mobile anion and (b) the probability distribution of mobile anions, $P(N_{\text{mobile}})$, as a function of the number of mobile anions, N_{mobile} . The curves are shifted vertically for visual clarity. Only a small proportion of the anions are mobile among the 400 total anions.

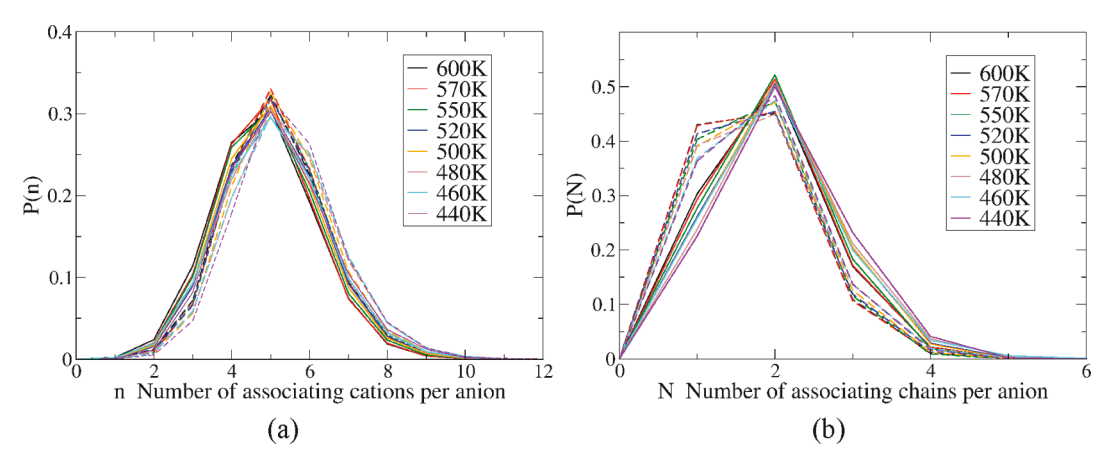


Figure 11. Comparison of the ion association environment of the mobile (solid lines) and immobile (dashed lines) anions. Probability of (a) the number of associating cations and (b) the number of associating chains. Mobile anions have relatively fewer associating cations from more associating chains than immobile ions.

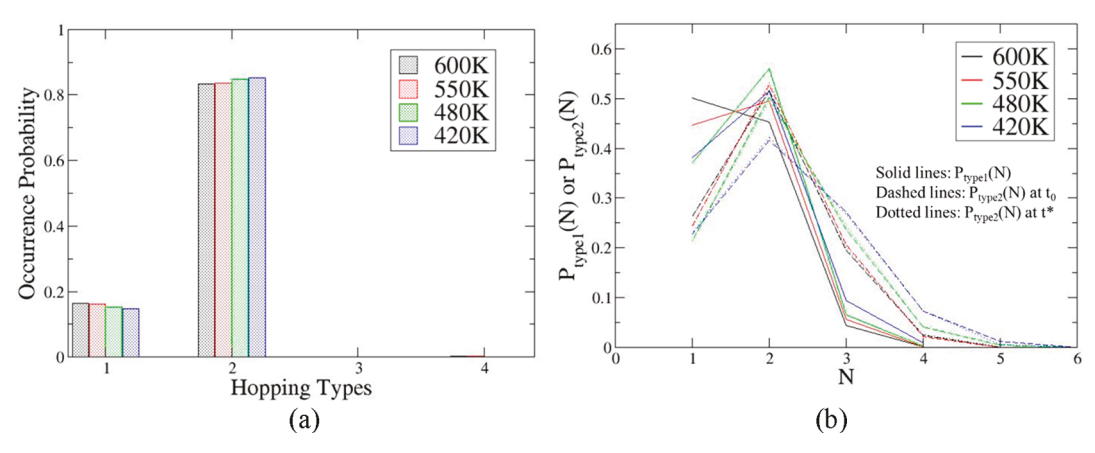


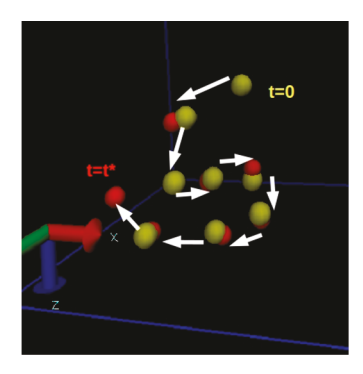
Figure 12. (a) Occurrence probability as a function of hopping type at four distinct temperatures. (b) Probability mass function for the hopping of mobile anions as a function of the number of chains, *N*. The hopping of the mobile anions is predominantly type 2, interchain ~85%. Type 1 intrachain hopping only accounts for about 15%.

the above equation. The representative concerted stringlike motion inside the simulation box is captured and shown as snapshots in Figure 13a. The white arrows show the path of the hopping and that the position of the ions at t = 0 are then occupied by the ions at $t = t^*$. This replacement is in a concerted manner forming the stringlike motion. In a recent investigation of Sokolov and co-workers, closed loops in the ion transport were hypothesized to explain the much slower ionic conductivity, 18 but this behavior was not observed directly in the simulations. Figure 13b shows the probability distribution of the string lengths, $P(n_s)$, but only the data points where $P(n_s)$ > 10⁻⁴ are plotted. The slow anions are artificially defined as the strings with "zero" length. It confirms that most of the anions are the slow ones, which are represented by the isolated points in the upper left corner with $n_s = 0$. Long strings with more than four anions are found, though the probabilities are much lower than observed with the short strings. Similar patterns of string length distribution were observed in the theoretical models for supercooled liquids, glass-forming liquids, and glass-forming polymer melts. 47,55,56 In this work, polyILs at higher temperatures tend to have shorter strings. The average string length $\langle n_s \rangle$ only counts in the strings with $n_s > 1$, which decreases with temperature except for the lowest temperature in the calculation. The exception is probably due to the slow dynamics at low temperatures that the ions are sufficiently mobile to form longer

strings. Generally, the observed increase in string length with decreasing temperature suggests that the apparent activation energy for anion transport increases in polyILs with decreasing temperature. The $\langle n_s \rangle$ for polyIL is about 1.6–2.2 depending on the temperature, which is consistent with $\langle n_s \rangle = 1.4-2.2$ for a theoretical supercooled liquid. Closed loops in the trajectory of the anions have not been positively identified and may therefore be elusive.

CONCLUSIONS

This work has performed the atomistic MD simulations for the polymerized ionic liquid, $poly(C_2VIm)Tf_2N$, and utilized multiple tools to analyze the ion hopping phenomenon. Ion hopping was initially investigated by using the traditional definition, which is based on the instant cation—anion association and dissociation within a time interval of 10 ps. About half of the anions are the hopping ions, and the intrachain hopping is dominant. The diffusivity was then calculated with the Einstein relation. However, the diffusivity was found to be the result of effective ion transport, which occurs at a longer time scale. Consequently, a new concept of effective hopping is introduced in that the anion must travel farther than a certain distance. The characteristic time scale of the effective hopping, t^* , was determined to be the time when the dynamical heterogeneity is the greatest. The distance criterion, r^* , was



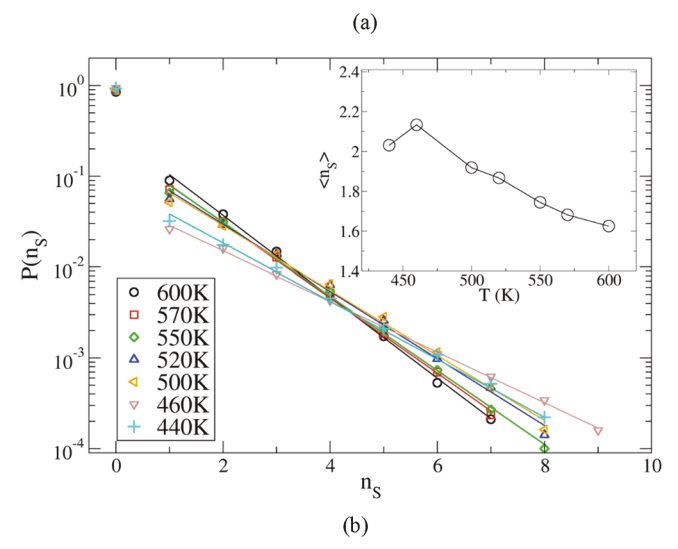


Figure 13. Stringlike motion. (a) A single string. The white arrows show the path. The yellow and red beads are the ions at t=0 and $t=t^*$. The string cutoff is adjusted to larger values to obtain longer strings for illustration. (b) The string length distribution. n_s is the string length, and $P(n_s)$ is its probability, with the solid lines of the exponential fit. Mobile anions tend to cooperatively move in a stringlike manner, but a considerable percentage of them only form very short strings. The average string length $\langle n_s \rangle$ generally decreases with temperature except at the lowest temperature.

determined from the self-part of the van Hove function, which shows multiple peaks. Using r^* and t^* , a reexamination of the dynamics revealed that only a small portion of the anions are mobile at this time, while most anions are just rattling around their original positions. This leads to the conclusion that the instant ion pair dissociation is not sufficient for effective hopping. Thus, the dissociation at a short time scale of picoseconds may be temporary, and the original association may be quickly recovered. "Half-shell" coordination and a "loose cage" of surrounded polymerized cations were discovered through visual inspection, which may be the structural basis for temporary dissociation.

Compared with the immobile anions, mobile anions have relatively fewer associating cations from the more associating chains. The types of hopping events are investigated again but only for mobile anions, and the sampling time was set to t^* , which is longer than the scale of ion-pair dissociation. We determined with our new analysis that interchain hopping is dominant among the effective hopping events. The motions of mobile anions were found to be correlated, and stringlike cooperative motion was observed, where the string length decreased with increasing temperature. Hence, proper identi-

fication of the principal mode of ion transport is significant in elucidating the mechanism of ion transport in polyILs. We hope our numerical observations will rationalize experimental observations and stimulate future experimental work in measuring the dynamical heterogeneity and cooperative motion. Our methods of analysis can be employed for other polyILs to investigate the effects of the chemistry, and the mechanistic findings in this work could shed some light on other single ion conductor systems.

ASSOCIATED CONTENT

Supporting Information

The Supporting Information is available free of charge at https://pubs.acs.org/doi/10.1021/acs.jpcb.0c06916.

Structural and ion association analysis; effect of structural and ion association relaxation on diffusivity; categorization of ion hopping types; and dynamical heterogeneity (PDF)

AUTHOR INFORMATION

Corresponding Author

Stephen J. Paddison — Department of Chemical and Biomolecular Engineering, University of Tennessee, Knoxville, Tennessee 37996, United States; orcid.org/0000-0003-1064-8233; Phone: +1 865-974-2026; Email: spaddison@utk.edu

Authors

Hongjun Liu — Department of Chemical and Biomolecular Engineering, University of Tennessee, Knoxville, Tennessee 37996, United States; orcid.org/0000-0003-3326-2640

Xubo Luo — Department of Chemical and Biomolecular Engineering, University of Tennessee, Knoxville, Tennessee 37996, United States; orcid.org/0000-0002-1591-7466

Alexei P. Sokolov — Department of Chemistry, University of Tennessee, Knoxville, Tennessee 37996, United States; Chemical Sciences Division, Oak Ridge National Laboratory, Oak Ridge, Tennessee 37831, United States; orcid.org/0000-0002-8187-9445

Complete contact information is available at: https://pubs.acs.org/10.1021/acs.jpcb.0c06916

Notes

The authors declare no competing financial interest.

ACKNOWLEDGMENTS

Financial support of the U.S. Army Research Office under Contracts W911NF-15-1-0501 and W911NF-16-1-0402 is gratefully acknowledged. Computing resources were provided through an XSEDE allocation DMR130078 on Stampede2 at the Texas Advanced Computing Center (TACC). A.P.S. acknowledges NSF support (CHE-1764409) for the data interpretation.

■ REFERENCES

- (1) Yuan, J.; Mecerreyes, D.; Antonietti, M. Poly(Ionic Liquid)s: An Update. *Prog. Polym. Sci.* **2013**, 38, 1009–1036.
- (2) Nishimura, N.; Ohno, H. 15th Anniversary of Polymerised Ionic Liquids. *Polymer* **2014**, *55*, 3289–3297.
- (3) Mecerreyes, D. Polymeric Ionic Liquids: Broadening the Properties and Applications of Polyelectrolytes. *Prog. Polym. Sci.* **2011**, *36*, 1629–1648.

- (4) Ohno, H.; Ito, K. Room-Temperature Molten Salt Polymers as a Matrix for Fast Ion Conduction. *Chem. Lett.* **1998**, *27*, 751–752.
- (5) Armand, M.; Endres, F.; MacFarlane, D. R.; Ohno, H.; Scrosati, B. Ionic-Liquid Materials for the Electrochemical Challenges of the Future. In Materials For Sustainable Energy: A Collection of Peer-Reviewed Research and Review Articles from Nature Publishing Group; World Scientific: 2011; pp 129–137.
- (6) Choi, U. H.; Ye, Y.; Salas de la Cruz, D.; Liu, W.; Winey, K. I.; Elabd, Y. A.; Runt, J.; Colby, R. H. Dielectric and Viscoelastic Responses of Imidazolium-Based Ionomers with Different Counterions and Side Chain Lengths. *Macromolecules* **2014**, *47*, 777–790.
- (7) Salas-De La Cruz, D.; Green, M. D.; Ye, Y.; Elabd, Y. A.; Long, T. E.; Winey, K. I. Correlating Backbone-to-Backbone Distance to Ionic Conductivity in Amorphous Polymerized Ionic Liquids. *J. Polym. Sci., Part B: Polym. Phys.* **2012**, *50*, 338–346.
- (8) Osada, I.; de Vries, H.; Scrosati, B.; Passerini, S. Ionic-Liquid-Based Polymer Electrolytes for Battery Applications. *Angew. Chem., Int. Ed.* **2016**, *55*, 500–513.
- (9) Ye, Y.; Choi, J. H.; Winey, K. I.; Elabd, Y. A. Polymerized Ionic Liquid Block and Random Copolymers: Effect of Weak Microphase Separation on Ion Transport. *Macromolecules* **2012**, *45*, 7027–7035.
- (10) Fan, F.; Wang, Y.; Hong, T.; Heres, M. F.; Saito, T.; Sokolov, A. P. Ion Conduction in Polymerized Ionic Liquids with Different Pendant Groups. *Macromolecules* **2015**, *48*, 4461–4470.
- (11) Evans, C. M.; Bridges, C. R.; Sanoja, G. E.; Bartels, J.; Segalman, R. A. Role of Tethered Ion Placement on Polymerized Ionic Liquid Structure and Conductivity: Pendant versus Backbone Charge Placement. ACS Macro Lett. 2016, 5, 925–930.
- (12) Fan, F.; Wang, W.; Holt, A. P.; Feng, H.; Uhrig, D.; Lu, X.; Hong, T.; Wang, Y.; Kang, N. G.; Mays, J.; et al. Effect of Molecular Weight on the Ion Transport Mechanism in Polymerized Ionic Liquids. *Macromolecules* **2016**, *49*, 4557–4570.
- (13) Iacob, C.; Matsumoto, A.; Brennan, M.; Liu, H.; Paddison, S. J.; Urakawa, O.; Inoue, T.; Sangoro, J.; Runt, J. Polymerized Ionic Liquids: Correlation of Ionic Conductivity with Nanoscale Morphology and Counterion Volume. *ACS Macro Lett.* **2017**, *6*, 941–946.
- (14) Griffin, P. J.; Freyer, J. L.; Han, N.; Geller, N.; Yin, X.; Gheewala, C. D.; Lambert, T. H.; Campos, L. M.; Winey, K. I. Ion Transport in Cyclopropenium-Based Polymerized Ionic Liquids. *Macromolecules* **2018**, *51*, 1681–1687.
- (15) Qian, W.; Texter, J.; Yan, F. Frontiers in Poly(Ionic Liquid)s: Syntheses and Applications. *Chem. Soc. Rev.* **2017**, *46*, 1124–1159.
- (16) Delhorbe, V.; Bresser, D.; Mendil-Jakani, H.; Rannou, P.; Bernard, L.; Gutel, T.; Lyonnard, S.; Picard, L. Unveiling the Ion Conduction Mechanism in Imidazolium-Based Poly(Ionic Liquids): A Comprehensive Investigation of the Structure-to-Transport Interplay. *Macromolecules* **2017**, *50*, 4309–4321.
- (17) Sangoro, J. R.; Iacob, C.; Agapov, A. L.; Wang, Y.; Berdzinski, S.; Rexhausen, H.; Strehmel, V.; Friedrich, C.; Sokolov, A. P.; Kremer, F. Decoupling of Ionic Conductivity from Structural Dynamics in Polymerized Ionic Liquids. *Soft Matter* **2014**, *10*, 3536–3540.
- (18) Stacy, E. W.; Gainaru, C. P.; Gobet, M.; Wojnarowska, Z.; Bocharova, V.; Greenbaum, S. G.; Sokolov, A. P. Fundamental Limitations of Ionic Conductivity in Polymerized Ionic Liquids. *Macromolecules* **2018**, *51*, 8637–8645.
- (19) Gainaru, C.; Stacy, E. W.; Bocharova, V.; Gobet, M.; Holt, A. P.; Saito, T.; Greenbaum, S.; Sokolov, A. P. Mechanism of Conductivity Relaxation in Liquid and Polymeric Electrolytes: Direct Link between Conductivity and Diffusivity. *J. Phys. Chem. B* **2016**, *120*, 11074–11083
- (20) Zhang, Y.; Maginn, E. J. Direct Correlation between Ionic Liquid Transport Properties and Ion Pair Lifetimes: A Molecular Dynamics Study. *J. Phys. Chem. Lett.* **2015**, *6*, 700–705.
- (21) Abbott, L. J.; Frischknecht, A. L. Nanoscale Structure and Morphology of Sulfonated Polyphenylenes via Atomistic Simulations. *Macromolecules* **2017**, *50*, 1184–1192.
- (22) Bocharova, V.; Wojnarowska, Z.; Cao, P. F.; Fu, Y.; Kumar, R.; Li, B.; Novikov, V. N.; Zhao, S.; Kisliuk, A.; Saito, T.; et al. Influence of Chain Rigidity and Dielectric Constant on the Glass Transition

- Temperature in Polymerized Ionic Liquids. *J. Phys. Chem. B* **2017**, *121*, 11511–11519.
- (23) Mogurampelly, S.; Keith, J. R.; Ganesan, V. Mechanisms Underlying Ion Transport in Polymerized Ionic Liquids. *J. Am. Chem. Soc.* **2017**, *139*, 9511–9514.
- (24) Keith, J. R.; Mogurampelly, S.; Wheatle, B. K.; Ganesan, V. Influence of Side Chain Linker Length on Ion-Transport Properties of Polymeric Ionic Liquids. *J. Polym. Sci., Part B: Polym. Phys.* **2017**, *55*, 1718–1723.
- (25) Keith, J. R.; Mogurampelly, S.; Aldukhi, F.; Wheatle, B. K.; Ganesan, V. Influence of Molecular Weight on Ion-Transport Properties of Polymeric Ionic Liquids. *Phys. Chem. Chem. Phys.* **2017**, 19, 29134–29145.
- (26) Mogurampelly, S.; Ganesan, V. Ion Transport in Polymerized Ionic Liquid–Ionic Liquid Blends. *Macromolecules* **2018**, *51*, 9471–9483.
- (27) Keith, J. R.; Rebello, N. J.; Cowen, B. J.; Ganesan, V. Influence of Counterion Structure on Conductivity of Polymerized Ionic Liquids. *ACS Macro Lett.* **2019**, *8*, 387–392.
- (28) Zhang, Z.; Krajniak, J.; Keith, J. R.; Ganesan, V. Mechanisms of Ion Transport in Block Copolymeric Polymerized Ionic Liquids. *ACS Macro Lett.* **2019**, *8*, 1096–1101.
- (29) Keith, J. R.; Ganesan, V. Ion Transport in Backbone-Embedded Polymerized Ionic Liquids. *J. Chem. Phys.* **2019**, *151*, 124902.
- (30) Pal, T.; Vogel, M. On the Relevance of Electrostatic Interactions for the Structural Relaxation of Ionic Liquids: A Molecular Dynamics Simulation Study. *J. Chem. Phys.* **2019**, *150*, 124501.
- (31) Liu, H.; Maginn, E. A Molecular Dynamics Investigation of the Structural and Dynamic Properties of the Ionic Liquid 1-n-Butyl-3-Methylimidazolium Bis(Trifluoromethanesulfonyl)Imide. *J. Chem. Phys.* **2011**, *135*, 124507.
- (32) Del Pópolo, M. G.; Voth, G. A. On the Structure and Dynamics of Ionic Liquids. *J. Phys. Chem. B* **2004**, *108*, 1744–1752.
- (33) Jiang, W.; Yan, T.; Wang, Y.; Voth, G. A. Molecular Dynamics Simulation of the Energetic Room-Temperature Ionic Liquid,1-Hydroxyethyl-4-Amino-1,2,4-Triazolium Nitrate (HEATN). *J. Phys. Chem. B* **2008**, *112*, 3121–3131.
- (34) Wang, Y.; Jiang, W.; Yan, T.; Voth, G. A. Understanding Ionic Liquids through Atomistic and Coarse-Grained Molecular Dynamics Simulations. *Acc. Chem. Res.* **2007**, *40*, 1193–1199.
- (35) Lu, K.; Maranas, J. K.; Milner, S. T. Ion-Mediated Charge Transport in Ionomeric Electrolytes. *Soft Matter* **2016**, *12*, 3943–3954.
- (36) Lin, K.-J.; Maranas, J. K. Superionic Behavior in Polyethylene-Oxide—Based Single-Ion Conductors. *Phys. Rev. E* **2013**, *88*, 052602.
- (37) Liu, H.; Paddison, S. J. Direct Comparison of Atomistic Molecular Dynamics Simulations and X-Ray Scattering of Polymerized Ionic Liquids. *ACS Macro Lett.* **2016**, *5*, 537–543.
- (38) Liu, H.; Paddison, S. J. Alkyl Chain Length Dependence of Backbone-to-Backbone Distance in Polymerized Ionic Liquids: An Atomistic Simulation Perspective on Scattering. *Macromolecules* **2017**, 50, 2889–2895.
- (39) Sprenger, K. G.; Jaeger, V. W.; Pfaendtner, J. The General AMBER Force Field (GAFF) Can Accurately Predict Thermodynamic and Transport Properties of Many Ionic Liquids. *J. Phys. Chem. B* **2015**, 119, 5882–5895.
- (40) Green, M. D.; Salas-De La Cruz, D.; Ye, Y.; Layman, J. M.; Elabd, Y. A.; Winey, K. I.; Long, T. E. Alkyl-Substituted N-Vinylimidazolium Polymerized Ionic Liquids: Thermal Properties and Ionic Conductivities. *Macromol. Chem. Phys.* **2011**, *212*, 2522–2528.
- (41) Nakamura, K.; Saiwaki, T.; Fukao, K. Dielectric Relaxation Behavior of Polymerized Ionic Liquid. *Macromolecules* **2010**, *43*, 6092–6098.
- (42) Abraham, M. J.; van der Spoel, D.; Lindahl, E.; Hess, B. GROMACS_development_team. GROMACS User Manual ver. 2019, www.gromacs.org (accessed June 14, 2020).
- (43) Liu, H.; Maginn, E.; Visser, A. E.; Bridges, N. J.; Fox, E. B. Thermal and Transport Properties of Six Ionic Liquids: An Experimental and Molecular Dynamics Study. *Ind. Eng. Chem. Res.* **2012**, *51*, 7242–7254.

- (44) Zhao, W.; Leroy, F.; Heggen, B.; Zahn, S.; Kirchner, B.; Balasubramanian, S.; Müller-Plathe, F. Are There Stable Ion-Pairs in Room-Temperature Ionic Liquids? Molecular Dynamics Simulations of 1- n -Butyl-3-Methylimidazolium Hexafluorophosphate. *J. Am. Chem. Soc.* 2009, 131, 15825–15833.
- (45) Bollinger, J. A.; Stevens, M. J.; Frischknecht, A. L. Quantifying Single-Ion Transport in Percolated Ionic Aggregates of Polymer Melts. *ACS Macro Lett.* **2020**, *9*, 583–587.
- (46) Kob, W.; Donati, C.; Plimpton, S. J.; Poole, P. H.; Glotzer, S. C. Dynamical Heterogeneities in a Supercooled Lennard-Jones Liquid. *Phys. Rev. Lett.* **1997**, *79*, 2827–2830.
- (47) Donati, C.; Douglas, J. F.; Kob, W.; Plimpton, S. J.; Poole, P. H.; Glotzer, S. C. Stringlike Cooperative Motion in a Supercooled Liquid. *Phys. Rev. Lett.* **1998**, *80*, 2338–2341.
- (48) Haddadian, E. J.; Zhang, H.; Freed, K. F.; Douglas, J. F. Comparative Study of the Collective Dynamics of Proteins and Inorganic Nanoparticles. *Sci. Rep.* **2017**, *7*, 41671.
- (49) Starr, F. W.; Douglas, J. F.; Sastry, S. The Relationship of Dynamical Heterogeneity to the Adam-Gibbs and Random First-Order Transition Theories of Glass Formation. *J. Chem. Phys.* **2013**, *138*, 12A541.
- (50) Shafique, N.; Kennedy, K. E.; Douglas, J. F.; Starr, F. W. Quantifying the Heterogeneous Dynamics of a Simulated Dipalmitoylphosphatidylcholine (DPPC) Membrane. *J. Phys. Chem. B* **2016**, *120*, 5172–5182.
- (51) Falck, E.; Róg, T.; Karttunen, M.; Vattulainen, I. Lateral Diffusion in Lipid Membranes through Collective Flows. *J. Am. Chem. Soc.* **2008**, *130*, 44–45.
- (52) Hanakata, P. Z.; Douglas, J. F.; Starr, F. W. Interfacial Mobility Scale Determines the Scale of Collective Motion and Relaxation Rate in Polymer Films. *Nat. Commun.* **2014**, *5*, 1–8.
- (53) Androulaki, E.; Vergadou, N.; Economou, I. G. Analysis of the Heterogeneous Dynamics of Imidazolium-Based [Tf2N-] Ionic Liquids Using Molecular Simulation. *Mol. Phys.* **2014**, *112*, 2694–2706.
- (54) Kelkar, M. S.; Maginn, E. J. Effect of Temperature and Water Content on the Shear Viscosity of the Ionic Liquid 1-Ethyl-3-Methylimidazolium Bis(Trifluoromethanesulfonyl)Imide As Studied by Atomistic Simulations † J. Phys. Chem. B 2007, 111, 4867–4876.
- (55) Donati, C.; Glotzer, S. C.; Poole, P. H.; Kob, W.; Plimpton, S. J. Spatial Correlations of Mobility and Immobility in a Glass-Forming Lennard-Jones Liquid. *Phys. Rev. E: Stat. Phys., Plasmas, Fluids, Relat. Interdiscip. Top.* **1999**, *60*, 3107–3119.
- (56) Gebremichael, Y.; Schrøder, T. B.; Starr, F. W.; Glotzer, S. C. Spatially Correlated Dynamics in a Simulated Glass-Forming Polymer Melt: Analysis of Clustering Phenomena. *Phys. Rev. E: Stat. Phys., Plasmas, Fluids, Relat. Interdiscip. Top.* **2001**, *64*, 051503.